THE JOURNAL OF PHYSICAL CHEMISTRY C
A JOURNAL OF THE AMERICAN CHEMICAL SOCIETY

pubs.acs.org/JPCC

Article

# Multiple Strategies to Approach High-Efficiency Luminescence Controllable in Blue/Cyan/Green-Emitting $Bi^{3+}$-Activated Phosphors

Peixin Gao, Qian Li, Siying Li, Shujie Gai, Yanan Li, Yibiao Ma, Zengtao Zhang, Maxim S. Molokeev, Zhi Zhou,* and Mao Xia*

Cite This: *J. Phys. Chem. C* 2022, 126, 9195−9206

Read Online

ACCESS | Metrics & More | Article Recommendations | Supporting Information

**ABSTRACT:** Cyan gap is a major block in achieving high-quality white light-emitting diodes (WLEDs). Hence, a novel cyan-emitting phosphor $Sr_2GdGaO_5/0.02Bi^{3+}$ with optical tuning performance is synthesized based on the local crystal field regulation strategy surrounding the luminescence center. With the substitution of $Al^{3+}$ for $Ga^{3+}$, the photoluminescence (PL) spectra of $Sr_2GdGa_{1-x}Al_xO_5/0.02Bi^{3+}$ ($0 \le x \le 1$) phosphors adjust from cyan (466 nm) to blue (450 nm). Moreover, such a $Ba^{2+}$ doping adjusts the PL spectra of $Sr_{2-x}Ba_xGdGaO_5/0.02Bi^{3+}$ ($0 \le x \le 0.5$) phosphors from cyan (466 nm) to green (482 nm). These phenomena are contributed to the crystal field splitting and nephelauxetic effect. The energy transfer from $Bi^{3+}$ to $Eu^{3+}$ is realized by co-doping $Bi^{3+}$ and $Eu^{3+}$ ions in the $A_2GdBO_5/Bi^{3+}$ (A = Sr, Ba; B = Ga, Al) host materials, and two single-phase white phosphors $Sr_2GdGaO_5/0.02Bi^{3+}$, $0.05Eu^{3+}$ and $Sr_{1.5}Ba_{0.5}GdGaO_5/0.02Bi^{3+}$, $0.05Eu^{3+}$ are obtained. Finally, a WLED with high color rendering index (Ra = 93.6) is prepared by using red/green/blue (RGB) phosphors and $Sr_2GdGaO_5/0.02Bi^{3+}$ phosphor, which is higher than that of the WLED prepared by RGB phosphors (Ra = 86.7), indicating that $Sr_2GdGaO_5/0.02Bi^{3+}$ phosphor can close the cyan gap. These results provide multiple strategies in achieving luminescence controllable and WLED.

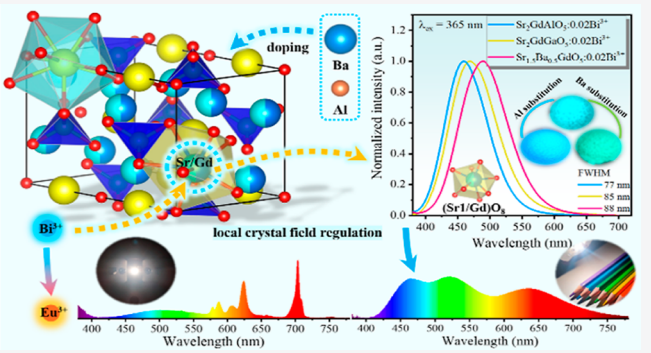


## INTRODUCTION

Recently, phosphor-converted white light-emitting diodes (pc-WLEDs) have attracted wide attention because of the advantages of high luminescence efficiency, long service life, and environmental friendliness and have become the main light source for illumination by degrees.[1−4] Currently, there are four common strategies to obtain pc-WLEDs, as follows: (1) blue light-emitting diode (LED) chips (470 nm) and $Y_3Al_5O_{12}/Ce^{3+}$ (YAG/Ce) yellow phosphor; (2) blue LED chips and red/green phosphors; (3) near ultraviolet (n-UV) LED chips (365 nm) and RGB phosphors; and (4) n-UV LED chips and white-emitting phosphors.[5−7] The first strategy is the easiest way to get white light, but the intense blue light produced by the blue LED chip can be harmful to the human eye.[8] Moreover, this combination of pc-WLED has a low Ra (<80) due to the lack of red and cyan light in the spectrum, which does not meet the requirements of high-quality white light illumination.[9−11] The second strategy also has the problem of intense blue light. It has been reported that n-UV LED chips + RGB phosphors (strategy three) is an effective method to solve the above problems, which can achieve whole-visible-spectrum white lighting.[12,13] However, this kind of pc-WLED still has the defect of cyan gap. If this problem can be solved, the lighting quality will undoubtedly be greatly improved.[14,15] Therefore, it is necessary to develop a high-efficiency cyan-emitting phosphor to close the cyan gap.

Rare-earth elements ($Ce^{3+}$ and $Eu^{2+}$) have been widely reported to exhibit cyan-emitting in suitable crystal field environments,[16−19] such as $NaMgBO_3/Ce^{3+}$, $Ca_2LuZr_2(AlO_4)_3/Ce^{3+}$, $NaAl_{11}O_{17}/Eu^{2+}$, and $Rb_2CaPO_4F/Eu^{2+}$ phosphors.[20−23] These phosphors' peak wavelengths are between 470 and 490 nm, and they have excellent internal quantum efficiency (IQE). Xia et al. mentioned a cyan-emitting phosphor $Na_{0.5}K_{0.5}Li_3SiO_4/Eu^{2+}$ with high thermal stability that can enhance the Ra from 86 to 95.2.[24] However, as with most rare-earth luminescent materials, $Ce^{3+}$-activated and $Eu^{2+}$-activated phosphors exhibit reabsorption phenomenon, which leads to color distortion.[25] Zhou et al. reported a new type of rare-earth-free ultra-narrow-band cyan-emitting phosphor $KAl_{11}O_{17}/Mn^{2+}$ with full width at half-maximum (FWHM) of 23.5 nm, and this phosphor has anti-thermal

Received: April 13, 2022
Revised: May 5, 2022
Published: May 20, 2022

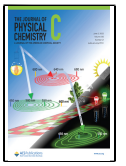







https://doi.org/10.1021/acs.jpcc.2c02560
*J. Phys. Chem. C* 2022, 126, 9195−9206

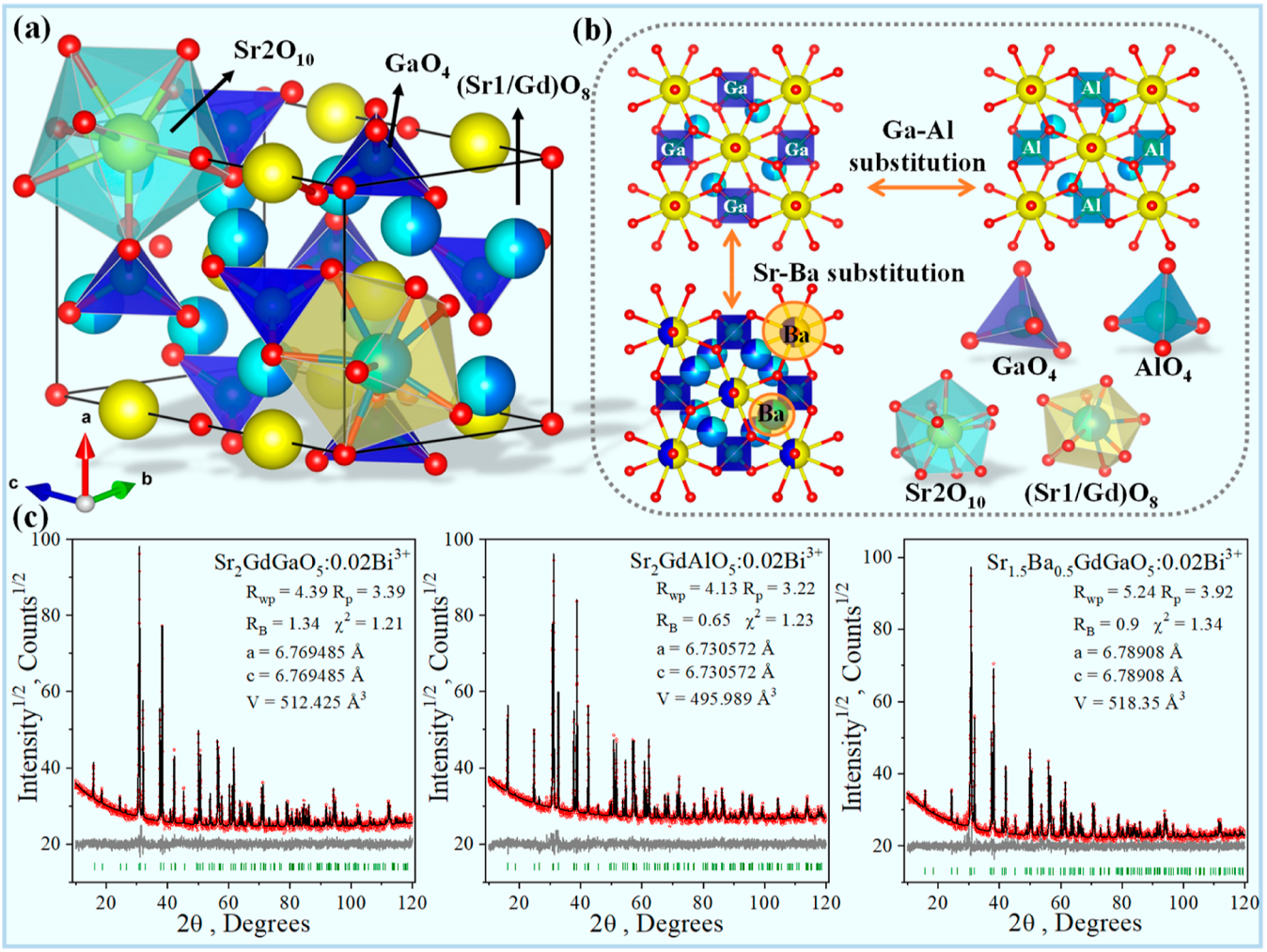


**Figure 1.** (a) Crystal structure diagram of $Sr_2GdGaO_5$ host material. (b) Schematic diagram of the local crystal field regulation design strategy ($Al^{3+}$ displaces $Ga^{3+}$, and $Ba^{2+}$ displaces $Sr^{2+}$). (c) Rietveld refinements of the powder XRD patterns of $Sr_2GdGaO_5/0.02Bi^{3+}$, $Sr_2GdAlO_5/0.02Bi^{3+}$, and $Sr_{1.5}Ba_{0.5}GdGaO_5/0.02Bi^{3+}$ phosphors.

quenching performance (130.4% at 150 °C) and high IQE = 71.3%.[26] Nevertheless, the optimal excitation peaks of $Na_{0.5}K_{0.5}Li_3SiO_4/Eu^{2+}$ and $KAl_{11}O_{17}/Mn^{2+}$ phosphors are located in the blue light region (400−460 nm), which does not correspond to the desired excitation band in the n-UV region.

Trivalent bismuth ion ($Bi^{3+}$), as a new type of non-rare-earth activator ion, has a strong absorption band in the ultraviolet region originating from the 6s → 6p transition, which can effectively avoid the reabsorption phenomenon in the visible region.[27−29] Furthermore, the luminescence behaviors of $Bi^{3+}$ ions are sensitive to crystal field environment due to the exposed 6s and 6p electrons, the versatile color output of blue ($Ca_3Lu_2Ge_3O_{12}/Bi^{3+}$),[30] cyan ($Ca_3Ga_4O_9/Bi^{3+}$),[31] green ($Ba_2LaGaO_5/Bi^{3+}$),[32] yellow ($Ba_2YGaO_5/Bi^{3+}$),[33] red ($K_2MgGeO_6/Bi^{3+}$),[34] and even near-infrared light [$XAl_{12}O_{19}/Bi^{3+}$ (X = Ba, Sr, and Ca)][35] could be achieved. Cyan-emitting is a special emission band of ions and is often used to compensate for the cyan gap in white-light illumination.[31] In the ultraviolet band, 365 nm n-UV chips are the most common. Therefore, in order to achieve commercial use, the photoluminescence excitation (PLE) wavelength of phosphors needs to be closer to 365 nm.[36,37] However, the excitation peaks of $Bi^{3+}$-activated phosphors are still unsatisfactory. Many $Bi^{3+}$-activated cyan-emitting phosphors' excitation peaks are located at nearly 310 nm, such as $BaSrGa_4O_8/Bi^{3+}$ ($\lambda_{ex}$ = 325 nm),[38] $K_2Ca_2Si_2O_7/Bi^{3+}$ ($\lambda_{ex}$ = 309 nm),[39] and $KGaGeO_4/Bi^{3+}$ ($\lambda_{ex}$ = 320 nm),[40] which do not match the n-UV chips well. Hence, it is necessary to develop a cyan-emitting phosphor with suitable PLE spectrum. Besides, $Bi^{3+}$ ion and $Eu^{3+}$ ion are usually acting as the activators of single-phase white-emitting phosphors, which are ascribed to the energy transfer from $Bi^{3+}$ (blue/cyan/green emission) to $Eu^{3+}$ (red emission).[27,32,41] The luminescence controllable from blue/cyan/green to red can achieve adjustable correlated color temperature (CCT) and can be used in plant fill-in lights.

Herein, we prepared a novel cyan-emitting phosphor $Sr_2GdGaO_5/0.02Bi^{3+}$ with a high IQE of 61.1% via the high-temperature solid-state method. Based on the local crystal field regulation strategy, $Al^{3+}$ and $Ba^{2+}$ were used to occupy $Ga^{3+}$ and $Sr^{2+}$ sites, respectively. A series of luminescence tunable phosphors $Sr_2GdGa_{1-x}Al_xO_5/0.02Bi^{3+}$ ($0 \le x \le 1$) (450−466 nm) and $Sr_{2-x}Ba_xGdGaO_5/0.02Bi^{3+}$ ($0 \le x \le 0.5$) (466−482 nm) were obtained, which are ascribed to the nephelauxetic effect and crystal field splitting. Especially, temperature-dependent emission spectra demonstrated that the thermal stability was improved by 39.1% with $Al^{3+}$ doping, which was attributed to the increase in activation energy. In addition, $Eu^{3+}$


https://doi.org/10.1021/acs.jpcc.2c02560
J. Phys. Chem. C 2022, 126, 9195−9206

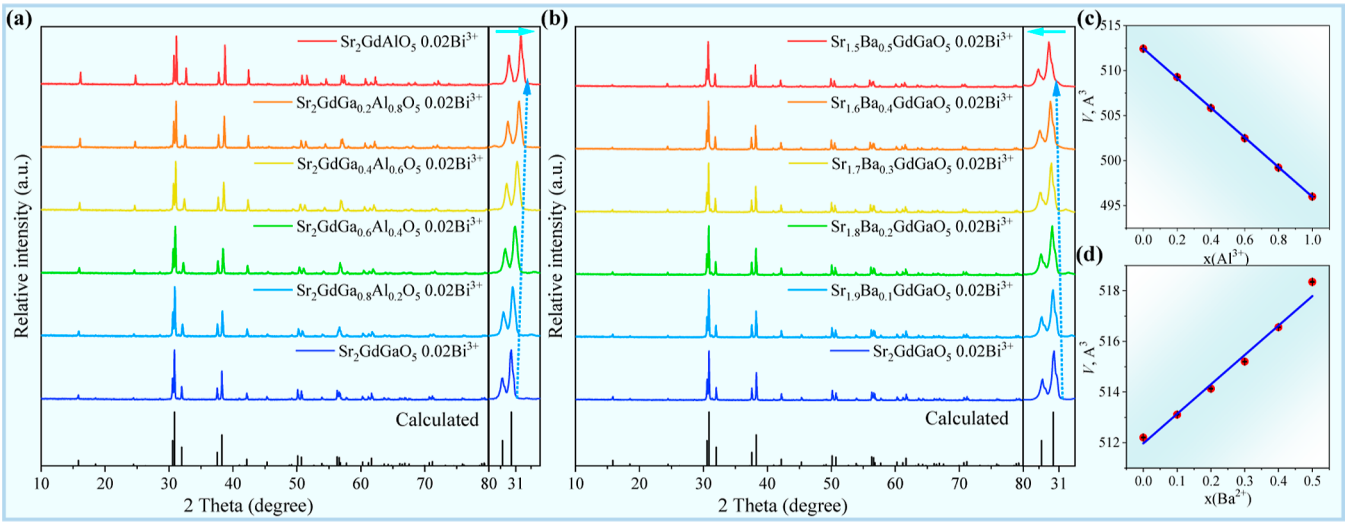


**Figure 2.** XRD patterns of (a) $Sr_2GdGa_{1-x}Al_xO_5/0.02Bi^{3+}$ and (b) $Sr_{2-x}Ba_xGdGaO_5/0.02Bi^{3+}$ phosphors. Linear cell volume dependence of (c) $Sr_2GdGa_{1-x}Al_xO_5/0.02Bi^{3+}$ and (d) $Sr_{2-x}Ba_xGdGaO_5/0.02Bi^{3+}$ phosphors.

ion was introduced to achieve the spectral tunability from blue/cyan/green to red emission. The energy-transfer process from $Bi^{3+}$ to $Eu^{3+}$ occurs in $Sr_2GdGaO_5/0.02Bi^{3+}$, $nEu^{3+}$, $Sr_2GdAlO_5/0.02Bi^{3+}$, $nEu^{3+}$, and $Sr_{1.5}Ba_{0.5}GdGaO_5/0.02Bi^{3+}$, $nEu^{3+}$ samples. A single-phase pc-WLED with low CCT = 3063 K was prepared by the $Sr_{1.5}Ba_{0.5}GdGaO_5/0.02Bi^{3+}$, $0.05Eu^{3+}$ phosphor. Finally, the cyan-emitting $Sr_2GdGaO_5/0.02Bi^{3+}$ phosphor was used to close the cyan gap to achieve whole-spectrum-lighting pc-WLED with excellent Ra = 93.6, indicating its potential application in WLED. Besides, the high-efficiency luminescence controllable phosphors have great significance in accurate plant lighting.

## EXPERIMENTAL SECTION

**Sample Synthesis.** All these samples were synthesized via the high-temperature solid-state method. The raw materials were $SrCO_3$ (99%), $BaCO_3$ (99%), $Gd_2O_3$ (99.99%), $Ga_2O_3$ (99.9%), $Al_2O_3$ (99.9%), and $Bi_2O_3$ (99.99%) and were weighted in stoichiometric proportions. Then, the raw materials were mixed with 2 mL of anhydrous ethanol in agate mortars and ground for 25 min. After that, the mixture was put in a 10 mL high purity corundum crucible and sintered in a muffle furnace at 1350 °C for 6 h. Finally, the samples were taken out and ground to a fine powder when the furnace cooled naturally to room temperature.

**Pc-LED Synthesis.** Three kinds of pc-WLEDs were prepared by $Sr_2GdGaO_5/0.02Bi^{3+}$, $Sr_2GdGaO_5/0.02Bi^{3+}$, $0.05Eu^{3+}$, and $Sr_{1.5}Ba_{0.5}GdGaO_5/0.02Bi^{3+}$, $0.05Eu^{3+}$ phosphors with 365 nm n-UV chips. First, a 600 mesh sieve was used to screen the phosphors to obtain finer particles. Then, the epoxy resin A and B were mixed uniformly in the ratio of 2:1. The well-mixed epoxy resin and phosphors were mixed and applied/coated evenly to the chips. Finally, the as-prepared pc-LEDs were placed in an oven at 90 °C for 18 h.

**Characterization.** PL and PLE spectra were measured using a F-4700 spectrometer (Hitachi, Japan), excited by a 150 W Xe lamp. The temperature-dependent PL spectra were tested on the same spectrometer coupled with a heat controller (Orient KOJI). X-ray diffraction (XRD) data were collected on an Aeris X-ray diffractometer (PANalytical, Netherlands). The operating condition was 40 kV and 15 mA, and the scanning ranges were 10−80 and 10−120°. The step size of 2-theta was 0.02°, and the counting time was 2 s per step. Diffuse reflectance (DR) spectra were tested on a Shimadzu ultraviolet spectrophotometer UV-2600 (Japan) with the range of 200 to 800 nm. PL decay times and quantum efficiency (QE) were recorded using a FLS920 spectrometer (Edinburgh, UK) and QE-2100 testing system (Otsuka, Japan), respectively. Electroluminescence (EL) spectra of pc-LEDs were obtained by an ATA-500 photoelectric test system (Everfine, China).

## RESULTS AND DISCUSSION

**Crystal Structure and Phase Identification.** Figure 1a displays the crystal structure of $Sr_2GdGaO_5$ host material, which belongs to tetragonal cell (*I*4/*mcm* space group).[42] Oxygen atoms connect with Sr, Gd, and Ga atoms to form $(Sr1/Gd)O_8$, $Sr2O_{10}$, and $GaO_4$ polyhedrons, respectively. It is well known that $Bi^{3+}$ tends to occupy eight coordination sites rather than four or ten coordination sites. Moreover, the ionic radii of $Bi^{3+}$ (CN = 8, $r$ = 1.17 Å) is closed to $Sr^{2+}$ (CN = 8, $r$ = 1.26 Å) and $Gd^{3+}$ (CN = 8, $r$ = 1.053 Å). Therefore, $Bi^{3+}$ ion is supposed to occupy the $(Sr1/Gd)O_8$ site.[43] Figure 1b shows the schematic diagram of the local crystal field regulation strategy. $Al^{3+}$ (CN = 4, $r$ = 0.39 Å) is closed to $Ga^{3+}$ (CN = 4, $r$ = 0.47 Å), and $Ba^{2+}$ (CN = 8 and 10, $r$ = 1.42 and 1.52 Å) is closed to $Sr^{2+}$ (CN = 8 and 10, $r$ = 1.26 and 1.44 Å), so $Al^{3+}$ and $Ba^{2+}$ tend to substitute $Ga^{3+}$ and $Sr^{2+}$ sites, which form a series of solid-solution materials $Sr_2GdGa_{1-x}Al_xO_5$ and $Sr_{2-x}Ba_xGdGaO_5$.

Figure S2 shows the XRD patterns of $Sr_2GdGaO_5/0.02Bi^{3+}$, $Sr_2GdAlO_5/0.02Bi^{3+}$, and $Sr_{1.5}Ba_{0.5}GdGaO_5/0.02Bi^{3+}$ phosphors. All peaks were indexed by the tetragonal cell (*I*4/*mcm*) with parameters close to $Sr_2GdGaO_5$.[42] The XRD Rietveld refinement of these three samples is displayed in Figure 1c. The low reliability factors (*R*-factors: $R_{wp}$, $R_p$, and $R_B$) and $\chi^2$ indicated that the refinement results are reliable. Figure 2 represents the XRD patterns of $Sr_2GdGa_{1-x}Al_xO_5/0.02Bi^{3+}$ ($0 \le x \le 1$) and $Sr_{2-x}Ba_xGdGaO_5/0.02Bi^{3+}$ ($0 \le x \le 0.5$) phosphors. All the peak positions are matched well with the calculated results, and the XRD patterns have no significant change, which illustrate that the crystal structures are similar, and the solid solutions are formed. Specially, the main


https://doi.org/10.1021/acs.jpcc.2c02560
J. Phys. Chem. C 2022, 126, 9195−9206

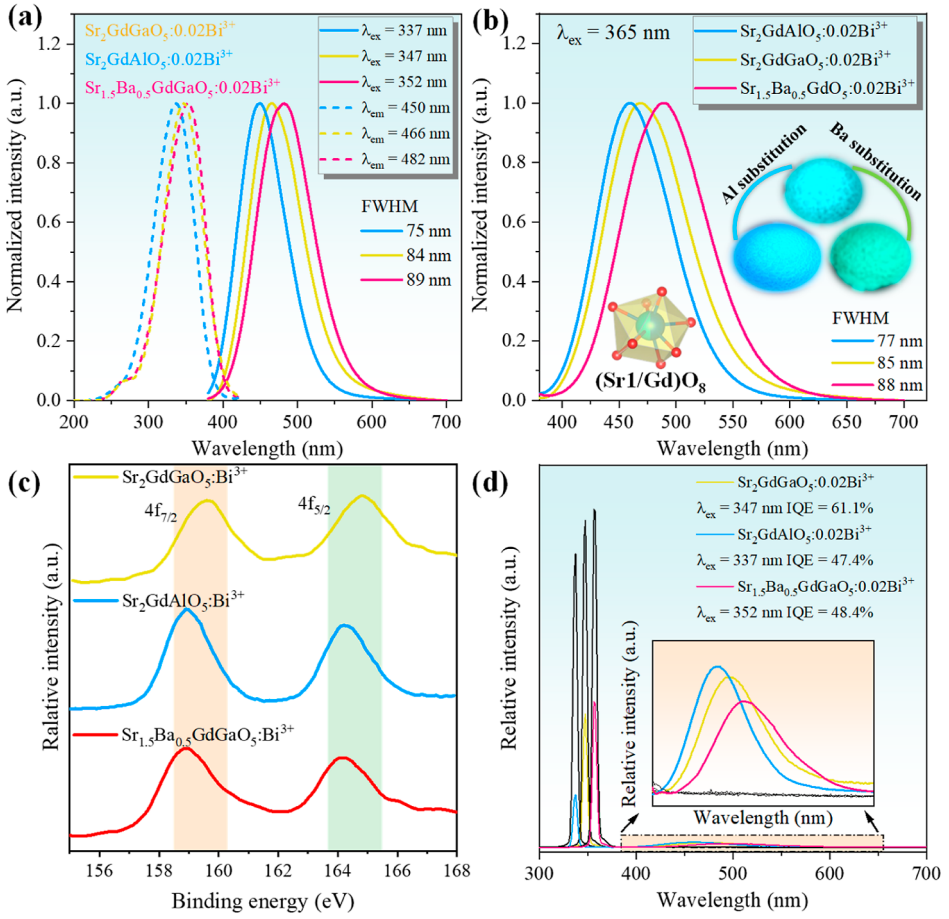


**Figure 3.** (a) Normalized intensity PLE and PL spectra, (b) normalized intensity PL spectra under 365 nm excitation, and (c) XPS spectra and (d) IQE of $Sr_2GdGaO_5/0.02Bi^{3+}$, $Sr_2GdAlO_5/0.02Bi^{3+}$, and $Sr_{1.5}Ba_{0.5}GdGaO_5/0.02Bi^{3+}$ phosphors.

**Table 1. Luminescence Parameters of $Sr_2GdGaO_5/0.02Bi^{3+}$, $Sr_2GdAlO_5/0.02Bi^{3+}$, and $Sr_{1.5}Ba_{0.5}GdGaO_5/0.02Bi^{3+}$ Phosphors**

| samples | $\lambda_{ex}$ (nm) | $\lambda_{em}$ (nm) | IQE/EQE | lifetime (ns) | $E_a$ (eV) |
|---|---|---|---|---|---|
| $Sr_2GdGaO_5/0.02Bi^{3+}$ | 337 | 450 | 61.1%/37.0% | 80.17 | 0.36 |
| $Sr_2GdAlO_5/0.02Bi^{3+}$ | 347 | 466 | 47.4%/39.2% | 78.02 | 0.40 |
| $Sr_{1.5}Ba_{0.5}GdGaO_5/0.02Bi^{3+}$ | 352 | 482 | 48.3%/28.0% | 72.21 | 0.37 |

diffraction peaks of $Sr_2GdGa_{1-x}Al_xO_5/0.02Bi^{3+}$ shift slightly to a large angle, as shown in the illustration of Figure 2a, which are attributed to the ion radii of $Al^{3+}$ (CN = 4, $r$ = 0.39 Å) smaller than that of $Ga^{3+}$ (CN = 4, $r$ = 0.47 Å). On the contrary, since the ion radii of $Ba^{2+}$ (CN = 8 and 10, $r$ = 1.42 and 1.52 Å) are larger than that of $Sr^{2+}$ (CN = 8 and 10, $r$ = 1.26 and 1.44 Å), the illustration in Figure 2b shows that the diffraction peaks of $Sr_{2-x}Ba_xGdGaO_5/0.02Bi^{3+}$ shift slightly to small angle with $Ba^{2+}$ substituting. As shown in Figure 2c,d, cell volume $V$ is decreasing with $x(Al^{3+})$ increasing and increasing with $x(Ba^{2+})$ increasing, which is consistent with the difference in ion radii. Linear cell volume dependence of $V(x)$ proves that suggested chemical compositions are close to real ones. The XRD Rietveld refinement patterns of $Sr_2GdGa_{1-x}Al_xO_5/0.02Bi^{3+}$ ($x$ = 0.0, 0.2, 0.4, 0.6, 0.8, and 1.0) and $Sr_{2-x}Ba_xGdGaO_5/0.02Bi^{3+}$ ($x$ = 0.0, 0.1, 0.2, 0.3, 0.4, and 0.5) phosphors are shown in Figures S3 and S4, and all the powder diffraction data are close to the calculated results. Tables S1 and S2 list the main parameters of processing and refinement of these samples. The low $R$-factors and $\chi^2$ indicated that all these samples are successfully synthesized. Besides, Tables S3 and S4 show the fractional atomic coordinates and isotropic displacement parameters (Å$^2$), and Tables S5 and S6 show the main band length (Å) of these samples.

**Photoluminescence Performance.** The intensity normalization PLE and PL spectra of $Sr_2GdGaO_5/0.02Bi^{3+}$, $Sr_2GdAlO_5/0.02Bi^{3+}$, and $Sr_{1.5}Ba_{0.5}GdGaO_5/0.02Bi^{3+}$ phosphors are shown in Figure 3a. These three phosphors present strong absorption in the n-UV region from 250 to 400 nm and peaks at 347, 337, and 352 nm, respectively. Under the excitation of the best excitation wavelengths, these phosphors ($Sr_2GdGaO_5/0.02Bi^{3+}$, $Sr_2GdAlO_5/0.02Bi^{3+}$, and $Sr_{1.5}Ba_{0.5}GdGaO_5/0.02Bi^{3+}$) exhibit narrow band emissions, with peaks located at 466, 450, and 482 nm, respectively. The emissions of these three phosphors are attributed to the luminescence center formed by $Bi^{3+}$ occupying the $(Sr1Gd)O_8$ site ($^3P_1 \rightarrow {}^1S_0$ transition of $Bi^{3+}$). In Figure 3b, upon excitation at 365 nm, $Sr_2GdGaO_5/0.02Bi^{3+}$ shows cyan emission with FWHM = 85 nm. With the substitution of $Al^{3+}$ and $Ba^{2+}$, the emitting color turns blue (FWHM = 77 nm) and green (FWHM = 88 nm). Figure 3c shows the X-ray


https://doi.org/10.1021/acs.jpcc.2c02560
J. Phys. Chem. C 2022, 126, 9195−9206

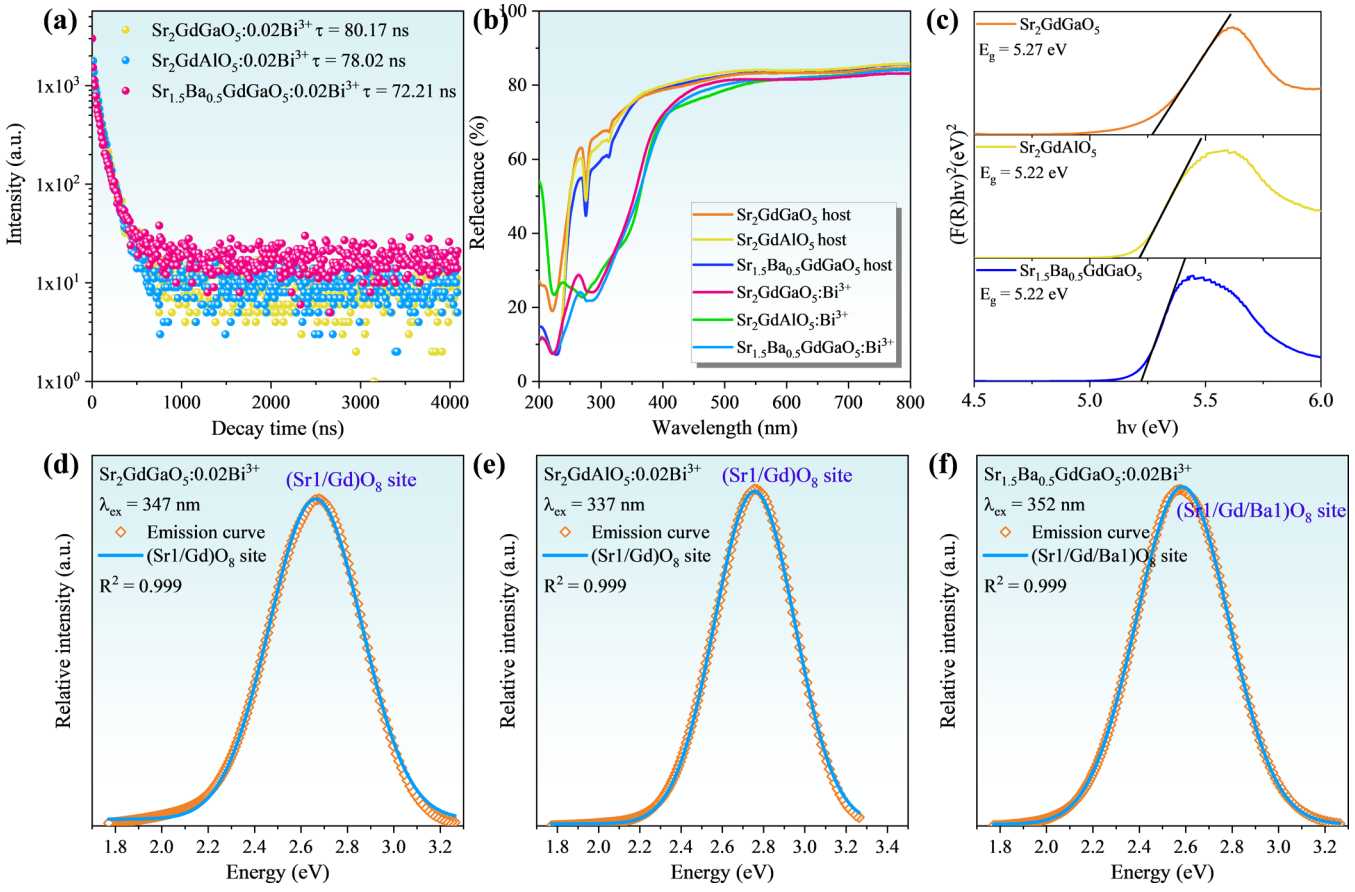


**Figure 4.** (a) PL decay curves of $Sr_2GdGaO_5/0.02Bi^{3+}$, $Sr_2GdAlO_5/0.02Bi^{3+}$, and $Sr_{1.5}Ba_{0.5}GdGaO_5/0.02Bi^{3+}$ phosphors monitoring at 450, 466, and 482 nm. (b) DR spectra of $Sr_2GdGaO_5$, $Sr_2GdAlO_5$, and $Sr_{1.5}Ba_{0.5}GdGaO_5$ host and representative $Bi^{3+}$-doped samples. (c) Calculated optical band gap values of $Sr_2GdGaO_5$, $Sr_2GdAlO_5$, and $Sr_{1.5}Ba_{0.5}GdGaO_5$ hosts. (d–f) Gaussian fitting of the PL spectra of $Sr_2GdGaO_5/0.02Bi^{3+}$, $Sr_2GdAlO_5/0.02Bi^{3+}$, and $Sr_{1.5}Ba_{0.5}GdGaO_5/0.02Bi^{3+}$ phosphors.

photoelectron spectra (XPS) of $Sr_2GdGaO_5/0.02Bi^{3+}$, $Sr_2GdAlO_5/0.02Bi^{3+}$, and $Sr_{1.5}Ba_{0.5}GdGaO_5/0.02Bi^{3+}$ phosphors. The characteristic peaks at about 159 and 164 eV are corresponding to $Bi^{3+4}f_{7/2}$ and $Bi^{3+4}f_{5/2}$, respectively, which suggest that these emissions originate from $Bi^{3+}$ ions. The peaks of $Bi^{3+4}f$ appear to slightly deviate with the substitution of $Al^{3+}$ and $Ba^{2+}$, which ascribed to the minor changes in the coordination environment of $Bi^{3+}$. QE is an important index to evaluate the luminescence performance of phosphors. The IQE and external QE (EQE) of these phosphors are displayed in Figure 3d and Table 1. The IQE/EQE of $Sr_2GdGaO_5/0.02Bi^{3+}$, $Sr_2GdAlO_5/0.02Bi^{3+}$, and $Sr_{1.5}Ba_{0.5}GdGaO_5/0.02Bi^{3+}$ phosphors is 61.1%/37.0%, 47.4%/39.2%, and 48.3%/28.0%, respectively, indicating the good luminescence performance.

The PL decay curves of these phosphors are shown in Figure 4a, and all these three curves could be fitted by a double exponential function as follows[44]

$$I(t) = I_0 + A_1 \exp\left(-\frac{t}{\tau_1}\right) + A_2 \exp\left(-\frac{t}{\tau_2}\right) \quad (1)$$

where $t$ represents the time, $\tau_1$ and $\tau_2$ are the exponential components of the lifetime. $I_0$ and $I(t)$ are the PL intensity at time 0 and time $t$, respectively. The average lifetime $\tau$ can be evaluated using the following equation[44]

$$\tau = \frac{A_1\tau_1^2 + A_2\tau_2^2}{A_1\tau_1 + A_2\tau_2} \quad (2)$$

where $A_1$ and $A_2$ are the constants and the average lifetimes of $Sr_2GdGaO_5/0.02Bi^{3+}$ (peaks at 466 nm), $Sr_2GdAlO_5/0.02Bi^{3+}$ (peaks at 450 nm), and $Sr_{1.5}Ba_{0.5}GdGaO_5/0.02Bi^{3+}$ (peaks at 482 nm) phosphors are 80.17, 78.02, and 72.21 ns, respectively. The lifetime variation is related to the phonon-induced transition probability between the ground state and the excited state. The different lifetime values of these phosphors proved the change in the coordination environment of $Bi^{3+}$ luminescence center. Figure 4b displays the DR spectra, and the band gap ($E_g$) of $Sr_2GdGaO_5$, $Sr_2GdAlO_5$ and $Sr_{1.5}Ba_{0.5}GdGaO_5$ samples are calculated, as shown in Figure 4c. According to the similar structure (Sr, Ba)$LaGaO_5$ reported previously, its band gap is direct band gap.[32] Therefore, the Kubelka–Munk absorption function was used to calculate the band gap[45] as follows[46,47]

$$F(R) = (1 - R)^2/2R \quad (3)$$

$$F(R)h\nu^2 = A(h\nu - E_g) \quad (4)$$

where $F(R)$, $R$, $h\nu$, and $E_g$ represent the absorption, reflection (%), photon energy, and band gap, respectively. The value of $E_g$ was obtained to be 5.27, 5.22, and 5.22 eV, indicating that the $Al^{3+}$ and $Ba^{2+}$ doping will lead to the decrease in the band gap. In conclusion, the change in these luminescence


https://doi.org/10.1021/acs.jpcc.2c02560
J. Phys. Chem. C 2022, 126, 9195−9206

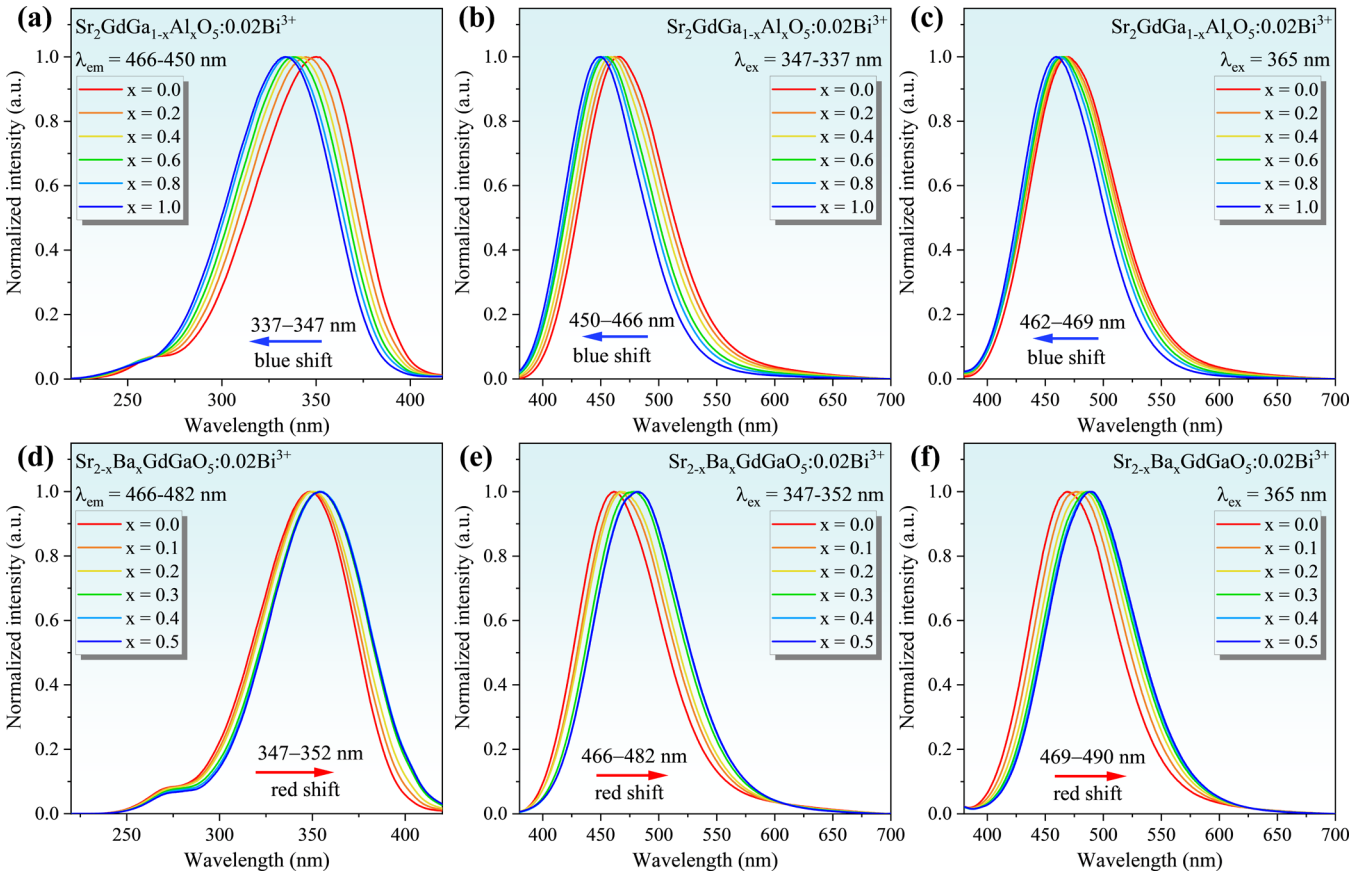


**Figure 5.** (a) Normalized PLE spectra of $Sr_2GdGa_{1-x}Al_xO_5/0.02Bi^{3+}$ phosphors ($\lambda_{em}$ = 450−466 nm). Normalized PL spectra of $Sr_2GdGa_{1-x}Al_xO_5/0.02Bi^{3+}$ phosphors (b) ($\lambda_{ex}$ = 337−347 nm) and (c) ($\lambda_{ex}$ = 365 nm). (d) Normalized PLE spectra of $Sr_{2-x}Ba_xGdGaO_5/0.02Bi^{3+}$ phosphors ($\lambda_{em}$ = 460−482 nm). Normalized PL spectra of $Sr_{2-x}Ba_xGdGaO_5/0.02Bi^{3+}$ phosphors (e) ($\lambda_{ex}$ = 347−352 nm) and (f) ($\lambda_{ex}$ = 365 nm).

parameters (Table 1) indicated that the local crystal field regulation strategy can effectively control the crystal field environment around the $Bi^{3+}$ ion luminescence center. To further confirm the occupied sites of $Bi^{3+}$ and the luminescence center, the Gaussian fitting of emission curves is given, as shown in Figure 4d−f. All these curves can fit well with one peak ($R^2$ = 0.999), implying that there is only one luminescence center and $Bi^{3+}$ occupies one site.

The relation of PL intensity and $Bi^{3+}$ concentration is illustrated in Figure S5. With $Bi^{3+}$ concentration increasing, the PL intensity increased first and then decreased due to the concentration quenching. Upon the optimal excitation wavelength, the PL intensity reached maximum when $x$ = 0.02. It shows that the PLE spectra present a red-shift, which is attributed to the variation in the surrounding crystal field caused by $Bi^{3+}$ concentration increasing. Figure 5 displays the normalized intensity PLE and PL spectra of $Sr_2GdGa_{1-x}Al_xO_5/0.02Bi^{3+}$ ($0 \le x \le 1$) and $Sr_{2-x}Ba_xGdGaO_5/0.02Bi^{3+}$ ($0 \le x \le 0.5$) phosphors. It is noticed that a blue-shift from 347 to 337 nm occurs in the PLE spectra with $Al^{3+}$ doping, as shown in Figure 5a. Meanwhile, the PL spectra also show a blue-shift from cyan (466 nm) to blue (450 nm) (Figure 5b). Nevertheless, as shown in Figure 5d−f, a red-shift from 466 to 482 nm was observed with the gradual doping of $Ba^{2+}$, which realized continuously controllable from cyan to green light. The optimum excitation wavelength transfer to 352 nm is closer to the commercial n-UV (365 nm) chip. When excited at 365 nm, the PL spectra present a red-shift from 469 to 490 nm (Figure 5f). In order to explain the blue-shift and red-shift phenomena, the crystal field strength ($D_q$) was introduced, and it can be calculated using the following equation[32,48]

$$D_q = \frac{1}{6} Ze^2 \frac{r^4}{R^5} \tag{5}$$

where $Z$ is the ligand ion charge, $e$ is the electron charge, and $r$ and $R$ represent the radius of the $d$ wave function and the band length, respectively. Theoretically, the bond length ($R$) is inversely proportional to the crystal field strength; the weaker the crystal field, the spectrum appears to be blue-shifted. Based on the Rietveld refinement (Tables S5 and S6), the average distance of Sr1/Gd−O and Sr1/Gd/Ba−O is calculated, as shown in Figure S6a,b. As for $Sr_2GdGa_{1-x}Al_xO_5/0.02Bi^{3+}$ samples, the average distance of Sr1/Gd−O decreases when $Al^{3+}$ gradually substitutes $Ga^{3+}$. According to the rules mentioned above, the emission spectra should show a red-shift trend, which is conflicting with the phenomenon of blue-shift. Besides, the average distance of Sr1/Gd/Ba−O changes irregularly, and the emission spectra shift toward red light. In addition to $R$ values, we introduced the lattice distortion degree ($D$), which also has a great impact on crystal field strength. Lattice distortion is closely related to crystal field splitting, resulting in the spectral shift. $D$ value was evaluated as follows[49,50]


https://doi.org/10.1021/acs.jpcc.2c02560
J. Phys. Chem. C 2022, 126, 9195−9206

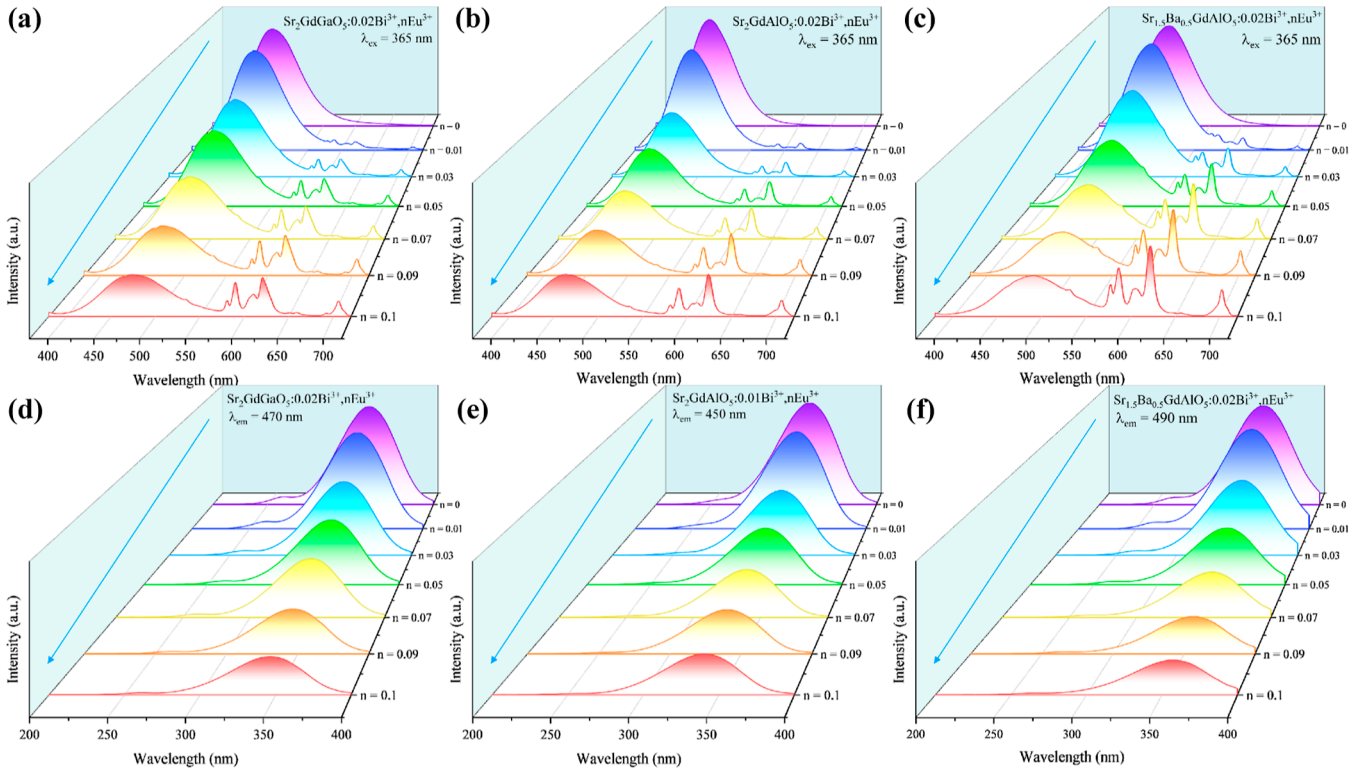


**Figure 6.** (a–c) PL spectra and (d–f) PLE spectra of $Sr_2GdGaO_5/0.02Bi^{3+}$, $nEu^{3+}$, $Sr_2GdAlO_5/0.02Bi^{3+}$, $nEu^{3+}$, and $Sr_{1.5}Ba_{0.5}GdGaO_5/0.02Bi^{3+}$, $nEu^{3+}$ phosphors.

$$D = \frac{1}{n}\sum_{i=0}^{n}\frac{|d_i - d_{av}|}{d_{av}} \quad (6)$$

Herein, $d_i$ and $d_{av}$ represent the band length and the average band length, respectively. In general, the larger the lattice distortion degree, the stronger the crystal field splitting, resulting in a red-shift phenomenon. The calculated results are displayed in Figure S6c,d. For $Sr_2GdGa_{1-x}Al_xO_5/0.02Bi^{3+}$ samples, the value of $D$ of the $(Sr1/Gd)O_8$ site decreases when $x$ increases, leading to the diminution of crystal field splitting and a blue-shift of the spectra. However, $D$ value of $(Sr1/Gd/Ba)O_8$ also changes irregularly. We speculated that the red-shift is caused by both crystal field strength and lattice distortion. In addition, the nephelauxetic effect also plays a key role in luminescence tuning. Because the electronegativity of $Sr^{2+}$ is higher than that of $Ba^{2+}$, the spectroscopic polarizability decreased with $Ba^{2+}$ substituting, resulting in the nephelauxetic effect, which leads to a red-shift phenomenon.[32] Figure S8 shows the photographs of $Sr_2GdGa_{1-x}Al_xO_5/0.02Bi^{3+}$ ($0 \le x \le 1$) and $Sr_{2-x}Ba_xGdGaO_5/0.02Bi^{3+}$ ($0 \le x \le 0.5$) phosphors under 365 nm UV lamps. It is obvious to observe the versatile color output from blue to cyan to green.

For blue/cyan/green $Bi^{3+}$-activated phosphors, it is a common method of constructing the energy transfer from $Bi^{3+}$ to $Eu^{3+}$ to achieve controllable luminescence and obtain single-phase white-emitting phosphor. Herein, a series of $Sr_2GdGaO_5/0.02Bi^{3+}$, $nEu^{3+}$, $Sr_2GdAlO_5/0.02Bi^{3+}$, $nEu^{3+}$, and $Sr_{1.5}Ba_{0.5}GdGaO_5/0.02Bi^{3+}$, $nEu^{3+}$ phosphors were prepared by introducing $Eu^{3+}$ ion. The XRD patterns showed that all the diffraction peaks matched well with the calculated results, indicating that the doping of $Eu^{3+}$ has almost no effect on the phase (Figure S9). Figure 6a–c show the PL spectra of $Sr_2GdGaO_5/0.02Bi^{3+}$, $nEu^{3+}$, $Sr_2GdAlO_5/0.02Bi^{3+}$, $nEu^{3+}$, and $Sr_{1.5}Ba_{0.5}GdGaO_5/0.02Bi^{3+}$, $nEu^{3+}$ phosphors ($\lambda_{ex}$ = 365 nm). All these PL spectra show $Bi^{3+}$ emissions ($^3P_1 \rightarrow {}^1S_0$ transition) and multiple narrowband emissions originated from $^5D_0 \rightarrow {}^7F_J$ ($J$ = 0, 1, 2, 3, and 4) transitions of $Eu^{3+}$. With the increase in the $Eu^{3+}$ concentration, $Bi^{3+}$ PL intensity gradually decreases while that of $Eu^{3+}$ increases, indicating the occurrence of energy transfer from $Bi^{3+}$ to $Eu^{3+}$. In addition to PL spectra, the PLE intensity of $Bi^{3+}$ also shows decreasing trends (Figure 6d–f). The CIE chromaticity coordinates were evaluated and are shown in Figure S10a. The coordinates move regularly with the change in the solid solution phase and $Eu^{3+}$ concentration. Figure S10b displays the photographs of corresponding phosphors under 365 nm n-UV lamps. These phosphors show various color outputs from blue/cyan/green emitting to origin/red emitting. Especially, $Sr_2GdGaO_5/0.02Bi^{3+}$, $0.05Eu^{3+}$ and $Sr_{1.5}Ba_{0.5}GdGaO_5/0.02Bi^{3+}$, $0.05Eu^{3+}$ phosphors present white-emitting, which can be used as candidate optical materials for single-phase WLED devices. To further verify the occurrence of energy transfer, the PL decay time of $Sr_2GdGaO_5/0.02Bi^{3+}$, $nEu^{3+}$ ($n$ = 0, 0.01, 0.05, and 0.09) were measured and are shown in Figure S11. On account of Formula 1 and 2, the decay time was calculated as 80.14, 75.77, 57.18, and 51.18 ns ($\lambda_{em}$ = 470 nm). The decreasing trend is in keeping with the emission of $Bi^{3+}$, which strongly evidenced the existence of energy transfer from $Bi^{3+}$ to $Eu^{3+}$. The efficiency of energy transfer can be obtained using the following equation[31,51,52]

$$\eta_T = 1 - \frac{\tau_n}{\tau_0} \quad (7)$$

$\tau_n$ and $\tau_0$ represent the lifetime value of $Bi^{3+}$ doped with and without $Eu^{3+}$, respectively. $\eta_T$ is the energy transfer efficiency, and the calculated results are 0, 5.4, 28.7, and 36.2%.



https://doi.org/10.1021/acs.jpcc.2c02560
J. Phys. Chem. C 2022, 126, 9195−9206

Therefore, the maximum efficiency was 36.2% when the concentration of $Eu^{3+}$ is 0.09. Figure 7 vividly depicts the luminescence mechanism of $Bi^{3+}$ and $Eu^{3+}$ and the energy transfer process between $Bi^{3+}$ and $Eu^{3+}$.

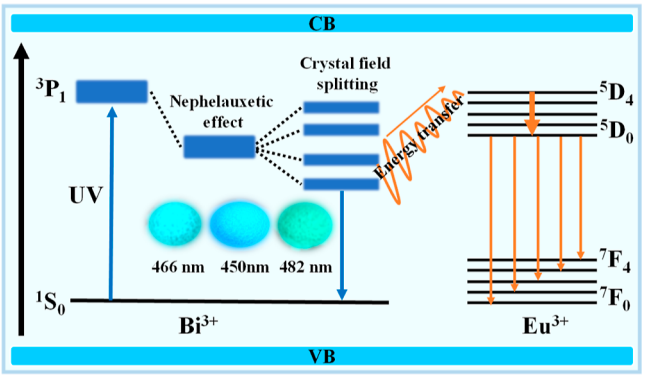


**Figure 7.** Schematic energy-level diagram for $Bi^{3+}$ ions and $Eu^{3+}$ ions in $Sr_2GdGaO_5/0.02Bi^{3+}$, $nEu^{3+}$, $Sr_2GdAlO_5/0.02Bi^{3+}$, $nEu^{3+}$, and $Sr_{1.5}Ba_{0.5}GdGaO_5/0.02Bi^{3+}$, $nEu^{3+}$ phosphors.

**Thermal Stability and WLED Applications.** The temperature-dependent emission spectra of $Sr_2GdGaO_5/0.02Bi^{3+}$, $Sr_2GdAlO_5/0.02Bi^{3+}$, and $Sr_{1.5}Ba_{0.5}GdGaO_5/0.02Bi^{3+}$ phosphors were measured and are shown in Figures 8a and S12. According to the diagram between integrated intensity and temperature (Figure 8b), all the emission intensities decrease with the temperature increasing due to the thermal quenching process. At 150 °C, the thermal quenching behavior of $Sr_2GdGaO_5/0.02Bi^{3+}$ and $Sr_{1.5}Ba_{0.5}GdGaO_5/0.02Bi^{3+}$ phosphors is similar, the PL intensities quenched over 70% of their initial intensities. When $Al^{3+}$ ion is introduced to occupy the $Ga^{3+}$ site, the downward trend has obviously reduced, and the PL intensity increased by 39% at 150 °C. The activation energy ($E_a$) of these three phosphors was obtained by Arrhenius equation fitting, and the formula is given as follows[36,53]

$$\ln[(I_0/I) - 1] = -\frac{E_a}{KT} + c \tag{8}$$

$I_0$ and $I$ represent the PL intensity at room temperature and temperature $T$, respectively. $K$ stands for the Boltzmann constant, and $c$ is a constant. The curve and linear fitting of $\ln(I_0/I - 1)$ and $1/kT$ are given in Figure 8d–f. $E_a$ values of $Sr_2GdGaO_5/0.02Bi^{3+}$, $Sr_2GdAlO_5/0.02Bi^{3+}$, and $Sr_{1.5}Ba_{0.5}GdGaO_5/0.02Bi^{3+}$ phosphors were calculated as 0.36, 0.40, and 0.37 eV, respectively. The increase in $E_a$ value proves the increase in thermal stability, which is consistent with the results. In addition, the reduction of cation radius results in better connection of the main lattice polyhedron and improves the structural rigidity, which leads to better thermal stability.[53] It is worth noting that the FWHM of these three phosphors widened with the increase in

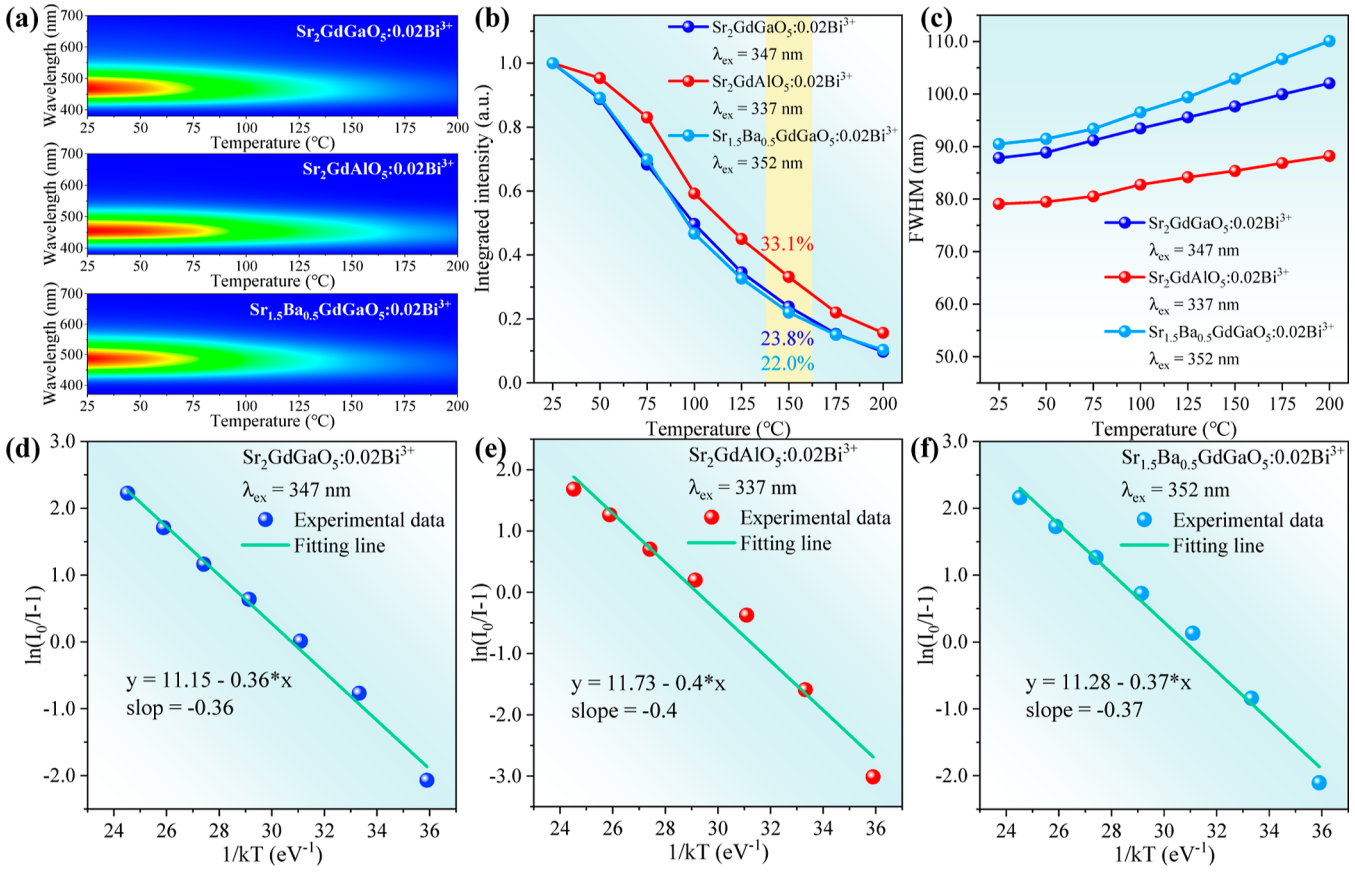


**Figure 8.** (a) Temperature-dependent PL spectra from 25 to 200 °C, (b) integrated emission intensity as a function of temperature, and (c) FWHM as a function of temperature of $Sr_2GdGaO_5/0.02Bi^{3+}$, $Sr_2GdAlO_5/0.02Bi^{3+}$, and $Sr_{1.5}Ba_{0.5}GdGaO_5/0.02Bi^{3+}$ phosphors. (d–f) Dependence of $\ln(I_0/I_T - 1)$ on $(-1/kT)$ according to the temperature-dependent PL spectra of $Sr_2GdGaO_5/0.02Bi^{3+}$, $Sr_2GdAlO_5/0.02Bi^{3+}$, and $Sr_{1.5}Ba_{0.5}GdGaO_5/0.02Bi^{3+}$ phosphors.



https://doi.org/10.1021/acs.jpcc.2c02560
J. Phys. Chem. C 2022, 126, 9195−9206

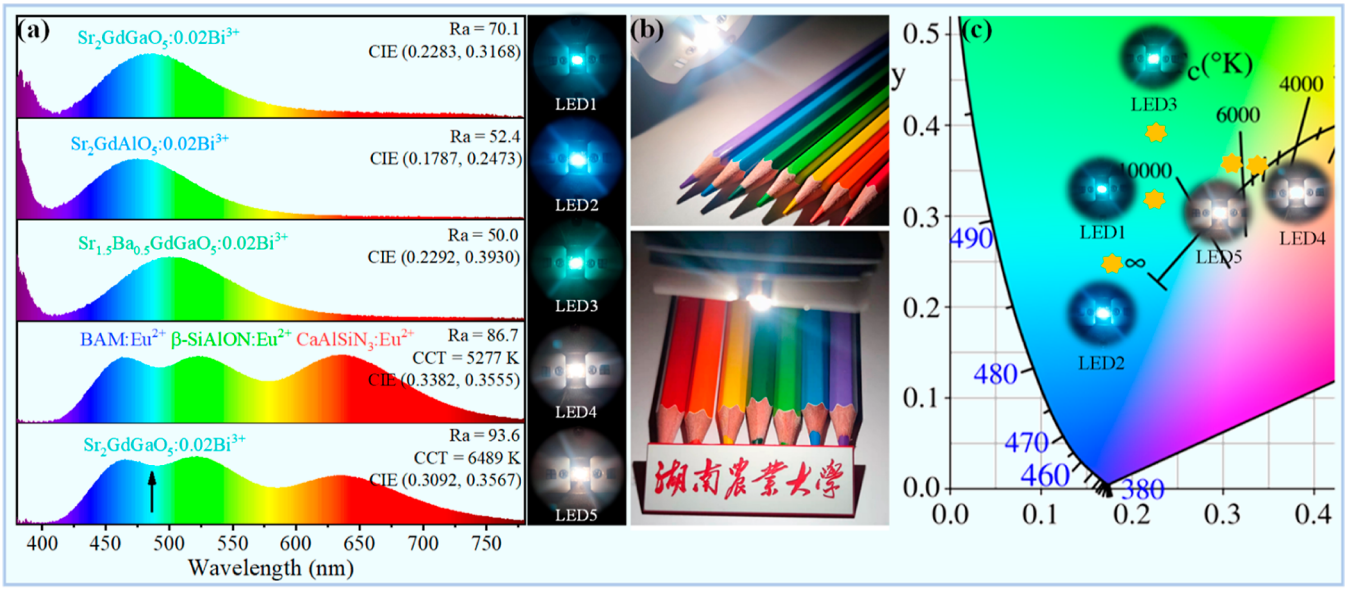


**Figure 9.** (a) EL spectra and luminescence photographs of the as-fabricated pc-LEDs. (b) Photographs of LED5 driven under a current of 200 mA. (c) CIE chromaticity coordinates of the as-fabricated pc-LEDs.

temperature (Figure 8c). Herein, the strength of the electron−lattice interaction [represented by the Huang-Rhys coupling parameter ($S$)] was introduced to explain this phenomenon; the formals are given as follows[50]

$$E_{\text{Stokes}} = (2S - 1)h\nu \tag{9}$$

$$\text{FWHM} = \sqrt{8 \ln 2} \times h\nu \times \sqrt{s} \times \sqrt{\coth\left(\frac{h\nu}{2kT}\right)} \tag{10}$$

where $E_{\text{stokes}}$ represents the energy for Stokes shift and $h\nu$ is the phonon energy. The higher the $S$ value, the stronger the electron−lattice interaction. Meanwhile, the $S$ value is proportional to the $E_{\text{stokes}}$ and $h\nu$, and FWHM connected with $S$ value and $h\nu$. Therefore, with increasing temperature, the FWHM increases. Besides, as shown in temperature-dependent normalized intensity PL spectra, different degrees of blue-shift of the three phosphors can be observed. This phenomenon is attributed to the thermal active phonon-assisted tunneling process. Meanwhile, at high temperature, the lattice expands, and the crystal field decreases, leading to the blue-shift of PL spectra.[31]

To assess the application prospect of these as-fabricated phosphors, the pc-LED devices were synthesized, and the EL spectra are shown in Figures 9 and S13. LED1−LED3 were fabricated by 365 nm n-UV chips and $Sr_2GdGaO_5/0.02Bi^{3+}$, $Sr_2GdAlO_5/0.02Bi^{3+}$, and $Sr_{1.5}Ba_{0.5}GdGaO_5/0.02Bi^{3+}$ phosphors, respectively. The CIE chromaticity coordinates were (0.2283, 0.3168), (0.1787, 0.2473), and (0.2292, 0.3930), respectively. WLED4 was combined by 365 nm n-UV chips and commercial RGB phosphors ($BaMgAl_{10}O_{17}/Eu^{2+}$, $\beta$-SiAlON/$Eu^{2+}$, and $CaAlSiN_3/Eu^{2+}$). Cyan-emitting phosphor $Sr_2GdGaO_5/0.02Bi^{3+}$ was added in commercial RGB phosphors to close the cyan gap (LED5), which has a higher Ra = 93.6 than that of LED4 (Ra = 86.7) and achieved high-quality WLED applications. Figure 9b exhibits some photographs of LED5 driven under a current of 200 mA, with characters and colored pencils clearly visible. As shown in Figure S13, LED6 and LED7 were prepared by single-phase white-emitting phosphors $Sr_2GdGaO_5/0.02Bi^{3+},0.05Eu^{3+}$ and $Sr_{1.5}Ba_{0.5}GdGaO_5/0.02Bi^{3+},0.05Eu^{3+}$. Both these exhibited warm white-emitting phosphors, and Commission Internationale de L'Eclairage (CIE) coordinates are (0.3458, 0.3331) and (0.4252, 0.3869), respectively. Compared with LED6 (Ra = 70.5 and CCT = 4898 K), LED7 has higher Ra = 79.3 and lower CCT = 3063, which is due to the wider band green light emission of $Sr_{1.5}Ba_{0.5}GdGaO_5/0.02Bi^{3+}$. All these results indicated the potential application of these phosphors in the field of WLED.

## CONCLUSIONS

In conclusion, a novel cyan-emitting phosphor $Sr_2GdGaO_5/0.02Bi^{3+}$ with IQE = 61.1% was synthesized via the high-temperature solid-state method. There was only one luminescent center, and $Bi^{3+}$ was supposed to occupy the $(Sr1/Gd)O_8$ site. Based on the local crystal field regulation strategy surrounding the luminescence center, a series of continuous luminescence controllable phosphors $Sr_2GdGa_{1-x}Al_xO_5/0.02Bi^{3+}$ and $Sr_{2-x}Ba_xGdGaO_5/0.02Bi^{3+}$ (tuning from 450 to 490 nm) were successfully prepared. XRD patterns and Rietveld refinements verified that these phosphors are pure and belong to the tetragonal cell ($I4/mcm$ space group). With the substitution of $Al^{3+}$ to $Ga^{3+}$, the thermal stability at 150 °C enhanced by 39% due to the increase in activation energy. The energy-transfer process from $Bi^{3+}$ to $Eu^{3+}$ was realized, and the PL spectra can be adjusted from blue/cyan/green to orange/red light. Finally, cyan-emitting phosphor $Sr_2GdGaO_5/0.02Bi^{3+}$ was utilized to close cyan gap and achieved high-quality WLED with a high Ra of 93.6. In addition, two warm white LED6 (Ra = 70.5, CCT = 4898 K) and LED7 (Ra = 79.3, CCT = 3063 K) were coated by single-phase white-emitting phosphors $Sr_2GdGaO_5/0.02Bi^{3+},0.05Eu^{3+}$ and $Sr_{1.5}Ba_{0.5}GdGaO_5/0.02Bi^{3+},0.05Eu^{3+}$ on 365 nm n-UV chips. Hence, the research results indicated that the local crystal field regulation strategy is an efficient method to realize luminescence controllable of $Bi^{3+}$, which has potential applications in WLED and accurate plant lighting.



https://doi.org/10.1021/acs.jpcc.2c02560
J. Phys. Chem. C 2022, 126, 9195−9206

## ■ ASSOCIATED CONTENT

### Supporting Information

The Supporting Information is available free of charge at https://pubs.acs.org/doi/10.1021/acs.jpcc.2c02560.

XRD patterns, Rietveld refinements results, main parameters of processing and refinement, average distance of Sr1/Gd−O and *D* values, temperature-dependent PL spectra, PL decay time, EL spectra, and CIE chromaticity coordinate (PDF)

## ■ AUTHOR INFORMATION


### Corresponding Authors

**Zhi Zhou** − *School of Chemistry and Materials Science, Hunan Agricultural University, Changsha 410128, P. R. China; Hunan Optical Agriculture Engineering Technology Research Center, Changsha 410128, P. R. China;* orcid.org/0000-0002-0547-506X; Phone: (+86)-13975160917; Email: zhouzhi@hunau.edu.cn

**Mao Xia** − *School of Chemistry and Materials Science, Hunan Agricultural University, Changsha 410128, P. R. China; Hunan Optical Agriculture Engineering Technology Research Center, Changsha 410128, P. R. China*; Phone: (+86)-15802612087; Email: xiamao2019@hunau.edu.cn

### Authors

**Peixin Gao** − *School of Chemistry and Materials Science, Hunan Agricultural University, Changsha 410128, P. R. China; Hunan Optical Agriculture Engineering Technology Research Center, Changsha 410128, P. R. China*

**Qian Li** − *School of Chemistry and Materials Science, Hunan Agricultural University, Changsha 410128, P. R. China; Hunan Optical Agriculture Engineering Technology Research Center, Changsha 410128, P. R. China*

**Siying Li** − *School of Chemistry and Materials Science, Hunan Agricultural University, Changsha 410128, P. R. China; Hunan Optical Agriculture Engineering Technology Research Center, Changsha 410128, P. R. China*

**Shujie Gai** − *Hunan Optical Agriculture Engineering Technology Research Center, Changsha 410128, P. R. China; College of Bioscience and Biotechnology, Hunan Agricultural University, Changsha 410128, P. R. China*

**Yanan Li** − *Hunan Optical Agriculture Engineering Technology Research Center, Changsha 410128, P. R. China; College of Bioscience and Biotechnology, Hunan Agricultural University, Changsha 410128, P. R. China*

**Yibiao Ma** − *School of Chemistry and Materials Science, Hunan Agricultural University, Changsha 410128, P. R. China; Hunan Optical Agriculture Engineering Technology Research Center, Changsha 410128, P. R. China*

**Zengtao Zhang** − *School of Chemistry and Materials Science, Hunan Agricultural University, Changsha 410128, P. R. China; Hunan Optical Agriculture Engineering Technology Research Center, Changsha 410128, P. R. China*

**Maxim S. Molokeev** − *Laboratory of Crystal Physics, Kirensky Institute of Physics, Federal Research Center KSC SB RAS, Krasnoyarsk 660036, Russia; Siberian Federal University, Krasnoyarsk 660041, Russia;* orcid.org/0000-0002-8297-0945

Complete contact information is available at: https://pubs.acs.org/10.1021/acs.jpcc.2c02560


### Author Contributions

P.G. and Q.L. contributed equally to this work. The manuscript was written through contributions of all authors. All authors have given approval to the final version of the manuscript.

### Notes

The authors declare no competing financial interest.

## ■ ACKNOWLEDGMENTS

The authors would like to gratefully acknowledge funds from the National Natural Science Foundation of China (grant no. 51974123), the Distinguished Youth Foundation of Hunan Province (grant no.2020JJ2018), the Key R&D projects in Hunan Province (2020WK2016, 2020SK2032, 2021SK2047, and 2022NK2044), the Natural Science Foundation of Hunan Province, China (grant no. 2021JJ40261), the Hunan High Level Talent Gathering Project (2019RS1077 and 2020RC5007), the Scientific Research Fund of Hunan Provincial Education Department (19C0903), the Natural Sciences Foundation of Hunan Agricultural University, China (grant no. 19QN11), the Hunan Provincial Key Laboratory of Crop Germplasm Innovation and Resource Utilization Science Foundation (19KFXM12), the Changsha Science and Technology Plan (KH2005114, KH2201428), and the College Students' Innovative Training (S202110537012).

## ■ REFERENCES


(1) Wei, Y.; Xing, G.; Liu, K.; Li, G.; Dang, P.; Liang, S.; Liu, M.; Cheng, Z.; Jin, D.; Lin, J. New strategy for designing orangish-red-emitting phosphor via oxygen-vacancy-induced electronic localization. *Light: Sci. Appl.* **2019**, *8*, 15−23.

(2) Zhao, M.; Yang, Z.; Ning, L.; Xia, Z. Tailoring of White Luminescence in a $NaLi_3SiO_4:Eu^{2+}$ Phosphor Containing Broad-Band Defect-Induced Charge-Transfer Emission. *Adv. Mater.* **2021**, *33*, 2101428−2101436.

(3) Cao, L.; Li, W.; Devakumar, B.; Ma, N.; Huang, X.; Lee, A. F. Full-Spectrum White Light-Emitting Diodes Enabled by an Efficient Broadband Green-Emitting $CaY_2ZrScAl_3O_{12}:Ce^{3+}$ Garnet Phosphor. *ACS Appl. Mater. Interfaces* **2022**, *14*, 5643−5652.

(4) Nair, G. B.; Swart, H. C.; Dhoble, S. J. A review on the advancements in phosphor-converted light emitting diodes (pc-LEDs): Phosphor synthesis, device fabrication and characterization. *Prog. Mater. Sci.* **2020**, *109*, 100622−100657.

(5) Zhu, H.; Feng, S.; Kong, Z.; Huang, X.; Peng, L.; Wang, J.; Wong, W.-Y.; Zhou, Z.; Xia, M. $Bi^{3+}$ occupancy rearrangement in $K_{2-x}A_xMgGeO_4$ phosphor to achieve ultra-broad-band white emission based on alkali metal substitution engineering. *Appl. Surf. Sci.* **2021**, *563*, 150252−150262.

(6) Song, M.; Ran, W.; Ren, Y.; Wang, L.; Zhao, W. Characterizations and photoluminescence properties of a dual-functional $La_2LiNbO_6:Bi^{3+}$, $Eu^{3+}$ phosphor for WLEDs and ratiometric temperature sensing. *J. Alloys Compd.* **2021**, *865*, 158825−158836.

(7) Wei, Y.; Yang, H.; Gao, Z.; Yun, X.; Xing, G.; Zhou, C.; Li, G. Anti-Thermal-Quenching $Bi^{3+}$ Luminescence in a Cyan-Emitting $Ba_2ZnGe_2O_7$:Bi Phosphor Based on Zinc Vacancy. *Laser Photonics Rev.* **2020**, *15*, 2000048−2000057.

(8) Xing, G.; Feng, Y.; Gao, Z.; Tao, M.; Wang, H.; Wei, Y.; Molokeev, M. S.; Li, G. A novel red-emitting $La_2CaHfO_6:Mn^{4+}$ phosphor based on double perovskite structure for pc-WLEDs lighting. *CrystEngComm* **2019**, *21*, 3605−3612.

(9) Wu, S.; Xiong, P.; Liu, X.; Fu, Y.; Liu, Q.; Chao, Y.; Dong, Q.; Li, Y.; Chen, W.; Chen, Y.; Ma, Z.; Peng, M.; et al. $Sr_3Y(BO_3)_3:Bi^{3+}$ phosphor with excellent thermal stability and color tunability for near-ultraviolet white-light LEDs. *J. Mater. Chem. C* **2021**, *9*, 3672−3681.

(10) Wu, S.; Xiong, P.; Liu, X.; Fu, Y.; Liu, Q.; Peng, M.; Chen, Y.; Ma, Z. Bismuth activated high thermal stability blue-emitting

phosphor $Na_2Y_2B_2O_7$:Bi used for near-UV white-light LEDs. *J. Mater. Chem. C* **2020**, *8*, 16584−16592.
(11) Zhong, Y.; Gai, S.; Yang, Y.; Xia, M.; Zhang, Y.; Qiu, F.; Xiang, F.; Zhou, Z. A novel green phosphor $Sr_8ZnY(PO_4)_7$:$Eu^{2+}$, $Ln^{3+}$ (Ln = Pr, Tm, Yb) with broad emission band for high color rendering white-lighting-emitting diodes. *J. Lumin.* **2019**, *214*, 116600−1146609.
(12) Wu, D.; Shi, C.; Zhou, J.; Gao, Y.; Huang, Y.; Ding, J.; Wu, Q. Full-visible-spectrum lighting enabled by site-selective occupation in the high efficient and thermal stable $(Rb, K)_2CaPO_4F$: $Eu^{2+}$ solid-solution phosphors. *Chem. Eng. J.* **2022**, *430*, 133062−133071.
(13) Zhao, D.; Li, Y.-N.; Zhang, R.-J.; Liu, B.-Z.; Yao, Q.-X. Tuning Emission from Greenish to Blue via Chemical Composition Modulation in Solid Solutions $(Sr_{1-y}Ca_y)_2Sb_2O_7$:$Bi^{3+}$ under near-UV Light Excitation. *ACS Sustainable Chem. Eng.* **2021**, *9*, 7569−7577.
(14) Sun, Q.; Wang, S.; Sun, L.; Liang, J.; Devakumar, B.; Huang, X. Achieving full-visible-spectrum LED lighting via employing an efficient $Ce^{3+}$-activated cyan phosphor. *Mater. Today Energy* **2020**, *17*, 100448−100455.
(15) Cai, M.; Lang, T.; Han, T.; Valiev, D.; Fang, S.; Guo, C.; He, S.; Peng, L.; Cao, S.; Liu, B.; Du, L.; Zhong, Y.; Polisadova, E.; et al. Novel Cyan-Green-Emitting $Bi^{3+}$-Doped $BaScO_2F$, $R^+$ (R = Na, K, Rb) Perovskite Used for Achieving Full-Visible-Spectrum LED Lighting. *Inorg. Chem.* **2021**, *60*, 15519−15528.
(16) Li, G.; Tian, Y.; Zhao, Y.; Lin, J. Recent progress in luminescence tuning of $Ce^{3+}$ and $Eu^{2+}$-activated phosphors for pc-WLEDs. *Chem. Soc. Rev.* **2015**, *44*, 8688−8713.
(17) Terraschke, H.; Wickleder, C. UV, Blue, Green Yellow, Red, and Small: Newest Developments on $Eu^{2+}$-Doped Nanophosphors. *Chem. Rev.* **2015**, *115*, 11352−11378.
(18) Liu, Y.; Silver, J.; Xie, R.-J.; Zhang, J.; Xu, H.; Shao, H.; Jiang, J.; Jiang, H. An excellent cyan-emitting orthosilicate phosphor for NUV-pumped white LED application. *J. Mater. Chem. C* **2017**, *5*, 12365−12377.
(19) Yao, Q.; Hu, P.; Sun, P.; Liu, M.; Dong, R.; Chao, K.; Liu, Y.; Jiang, J.; Jiang, H. YAG:$Ce^{3+}$ Transparent Ceramic Phosphors Brighten the Next-Generation Laser-Driven Lighting. *Adv. Mater.* **2022**, *32*, 1907888−1907894.
(20) Zhong, J.; Zhuo, Y.; Hariyani, S.; Zhao, W.; Wen, J.; Brgoch, J. Closing the Cyan Gap Toward Full-Spectrum LED Lighting with $NaMgBO_3$:$Ce^{3+}$. *Chem. Mater.* **2019**, *32*, 882−888.
(21) Sun, L.; Devakumar, B.; Liang, J.; Wang, S.; Sun, Q.; Huang, X. A broadband cyan-emitting $Ca_2LuZr_2(AlO_4)_3$:$Ce^{3+}$ garnet phosphor for near-ultraviolet-pumped warm-white light-emitting diodes with an improved color rendering index. *J. Mater. Chem. C* **2020**, *8*, 1095−1103.
(22) Shi, R.; Zhang, X.; Qiu, Z.; Zhang, J.; Liao, S.; Zhou, W.; Xu, X.; Yu, L.; Lian, S. Composition and Antithermal Quenching of Noninteger Stoichiometric $Eu^{2+}$-Doped Na-$\beta$-Alumina with Cyan Emission for Near-UV WLEDs. *Inorg. Chem.* **2021**, *60*, 19393−19401.
(23) Zhang, R.; Sun, J.-F. An efficient perovskite-type $Rb_2CaPO_4F$:$Eu^{2+}$ phosphor with high brightness towards closing the cyan gap. *J. Alloys Compd.* **2021**, *872*, 159698−159713.
(24) Zhao, M.; Liao, H.; Molokeev, M. S.; Zhou, Y.; Zhang, Q.; Liu, Q.; Xia, Z. Emerging ultra-narrow-band cyan-emitting phosphor for white LEDs with enhanced color rendition. *Light: Sci. Appl.* **2019**, *8*, 38−46.
(25) Xia, Z.; Meijerink, A. $Ce^{3+}$-Doped garnet phosphors: composition modification, luminescence properties and applications. *Chem. Soc. Rev.* **2017**, *46*, 275−299.
(26) Zhou, Z.; Zhu, H.; Huang, X.; She, Y.; Zhong, Y.; Wang, J.; Liu, M.; Li, W.; Xia, M. Anti-thermal-quenching, color-tunable and ultra-narrow-band cyan green-emitting phosphor for w-LEDs with enhanced color rendering. *Chem. Eng. J.* **2022**, *433*, 134079−134089.
(27) Dang, P.; Liu, D.; Li, G.; Al Kheraif, A. A.; Lin, J. Recent Advances in Bismuth Ion-Doped Phosphor Materials: Structure Design, Tunable Photoluminescence Properties, and Application in White LEDs. *Adv. Opt. Mater.* **2020**, *8*, 1901993−1902005.
(28) Yan, W.; Chen, S.; Liu, Y.; Gao, Z.; Wei, Y.; Li, G. Giant Photoluminescence Improvement and Controllable Emission Adjustment in $Bi^{3+}$-Activated $Ca_4ZrGe_3O_{12}$ Phosphors for HighQuality White Light-Emitting Diodes. *ACS Appl. Electron. Mater.* **2019**, *1*, 1970−1980.
(29) Wei, Y.; Li, G. Narrow-band Blue Emission of $Bi^{3+}$ Based on High Crystal Structure Symmetry. *Chin. J. Lumin.* **2021**, *42*, 1365−1375.
(30) Ye, S.; Liu, H.; Wang, Y.; Lin, J.; Zhong, K.; Ding, J.; Wu, Q. Design of a Bismuth-Activated Narrow-Band Cyan Phosphor for Use in White Light Emitting Diodes and Field Emission Displays. *ACS Sustainable Chem. Eng.* **2020**, *8*, 18187−18195.
(31) Liu, D.; Yun, X.; Li, G.; Dang, P.; Molokeev, M. S.; Lian, H.; Shang, M.; Lin, J. Enhanced Cyan Emission and Optical Tuning of $Ca_3Ga_4O_9$:$Bi^{3+}$ for High-Quality Full-Spectrum White Light-Emitting Diodes. *Adv. Opt. Mater.* **2020**, *8*, 2001037−2001049.
(32) Liu, D.; Dang, P.; Yun, X.; Li, G.; Lian, H.; Lin, J. Luminescence color tuning and energy transfer properties in $(Sr,Ba)_2LaGaO_5$:$Bi^{3+}$,$Eu^{3+}$ solid solution phosphors: realization of single-phased white emission for WLEDs. *J. Mater. Chem. C* **2019**, *7*, 13536−13547.
(33) Ye, S.; Ding, J.; Wu, Q. MMCT-induced high-bright yellow light-emitting phosphor $Bi^{3+}$-activated $Ba_2YGaO_5$ used for WLED. *Chem. Eng. J.* **2022**, *428*, 131128−131135.
(34) Li, H.; Pang, R.; Liu, G.; Sun, W.; Li, D.; Jiang, L.; Zhang, S.; Li, C.; Feng, J.; Zhang, H. Synthesis and Luminescence Properties of $Bi^{3+}$-Activated $K_2MgGeO_4$: A Promising High-Brightness Orange-Emitting Phosphor for WLEDs Conversion. *Inorg. Chem.* **2018**, *57*, 12303−12311.
(35) Wei, Y.; Gao, Z.; Yun, X.; Yang, H.; Liu, Y.; Li, G. Abnormal $Bi^{3+}$-Activated NIR Emission in Highly Symmetric $XAl_{12}O_{19}$ (X = Ba, Sr, Ca) by Selective Sites Occupation. *Chem. Mater.* **2020**, *32*, 8747−8753.
(36) Liu, D.; Yun, X.; Dang, P.; Lian, H.; Shang, M.; Li, G.; Lin, J. Yellow/Orange-Emitting $ABZn_2Ga_2O_7$:$Bi^{3+}$ (A = Ca, Sr; B = Ba, Sr) Phosphors: Optical Temperature Sensing and White Light-Emitting Diode Applications. *Chem. Mater.* **2020**, *32*, 3065−3077.
(37) Arfin, H.; Kaur, J.; Sheikh, T.; Chakraborty, S.; Nag, A. $Bi^{3+}$-$Ln^{3+}$ (Ln = Er and Yb) codoped $Cs_2AgInCl_6$ Double Perovskite Near Infrared Emitter. *Angew. Chem., Int. Ed.* **2020**, *59*, 11307−11311.
(38) Dang, P.; Liu, D.; Yun, X.; Li, G.; Huang, D.; Lian, H.; Shang, M.; Lin, J. Ultra-broadband cyan-to-orange emitting $Ba_{1+x}Sr_{1-x}Ga_4O_8$:$Bi^{3+}$ phosphors: luminescence control and optical temperature sensing. *J. Mater. Chem. C* **2020**, *8*, 1598−1607.
(39) Leng, Z.; Zhang, D.; Bai, H.; She, P.; Zhao, J.; Tang, Z. Site occupancy and photoluminescence properties of cyan-emitting $K_2Ca_2Si_2O_7$:$Bi^{3+}$ phosphor for white light emitting diodes. *Opt. Mater.* **2021**, *118*, 111293−111300.
(40) Sun, W.; Pang, R.; Li, H.; Li, D.; Jiang, L.; Zhang, S.; Fu, J.; Li, C. Investigation of a novel color tunable long afterglow phosphor $KGaGeO_4$:$Bi^{3+}$: luminescence properties and mechanism. *J. Mater. Chem. C* **2017**, *5*, 1346−1355.
(41) Shang, M.; Li, C.; Lin, J. How to produce white light in a single-phase host? *Chem. Soc. Rev.* **2014**, *43*, 1372−1386.
(42) Nguyen-trut-Dinh, M.; Fava, J.; Flem, G. L. Étude Structurale et Optique de La Phase $Sr_2GdGaO_5$ Dopée a L′ Europium Trivalent. *Z. Anorg. Allg. Chem.* **1977**, *433*, 275−283.
(43) Jia, Z.; Yuan, C.; Liu, Y.; Wang, X.-J.; Sun, P.; Wang, L.; Jiang, H.; Jiang, J. Strategies to approach high performance in $Cr^{3+}$-doped phosphors for high-power NIR-LED light sources. *Light: Sci. Appl.* **2020**, *9*, 86−94.
(44) Zhang, H.; Zhang, J.; Su, Y.; Zhang, X. Metal To Metal Charge Transfer Induced Efficient Yellow/Far-Red Luminescence in $Na_2Ca_3(Nb,Ta)_2O_9$:$Bi^{3+}$ toward the Applications of White-LEDs and Plant Growth Light. *Adv. Opt. Mater.* **2022**, *10*, 2200150−2200159.
(45) Zhang, L.; Wang, D.; Hao, Z.; Zhang, X.; Pan, G.; Wu, H.; Zhang, J. $Cr^{3+}$-Doped Broadband NIR Garnet Phosphor with


https://doi.org/10.1021/acs.jpcc.2c02560
J. Phys. Chem. C 2022, 126, 9195−9206

Enhanced Luminescence and its Application in NIR Spectroscopy. *Adv. Opt. Mater.* **2019**, *7*, 1900185−1900192.
(46) Ding, S.; Guo, H.; Feng, P.; Ye, Q.; Wang, Y. A New Near-Infrared Long Persistent Luminescence Material with Its Outstanding Persistent Luminescence Performance and Promising Multifunctional Application Prospects. *Adv. Opt. Mater.* **2020**, *8*, 2000097−2000108.
(47) Lang, T.; Cai, M.; Fang, S.; Han, T.; He, S.; Wang, Q.; Ge, G.; Wang, J.; Guo, C.; Peng, L.; Cao, S.; Liu, B.; Korepanov, V. I.; Yakovlev, A. N.; Qiu, J.; et al. Trade-off Lattice Site Occupancy Engineering Strategy for Near-Infrared Phosphors with Ultrabroad and Tunable Emission. *Adv. Opt. Mater.* **2021**, *10*, 2101633−2101644.
(48) Zhang, X.; An, Z.; Dong, R.; Song, Y.; Zheng, K.; Sheng, Y.; Shi, Z.; Zou, H. Properties and Application of Single $Eu^{2+}$-Activated Color Tuning Phosphors. *ACS Sustainable Chem. Eng.* **2019**, *7*, 10724−10733.
(49) Wei, Y.; Dang, P.; Dai, Z.; Li, G.; Lin, J. Advances in Near-Infrared Luminescent Materials without $Cr^{3+}$: Crystal Structure Design, Luminescence Properties, and Applications. *Chem. Mater.* **2021**, *33*, 5496−5526.
(50) Dang, P.; Zhang, Q.; Liu, D.; Li, G.; Lian, H.; Shang, M.; Lin, J. Hetero-valent substitution strategy toward orange-red luminescence in $Bi^{3+}$ doped layered perovskite oxide phosphors for high color rendering index white light-emitting diodes. *Chem. Eng. J.* **2021**, *420*, 127640−127649.
(51) Liu, G.; Hu, T.; Molokeev, M. S.; Xia, Z. Li/Na substitution and $Yb^{3+}$ co-doping enabling tunable near-infrared emission in $LiIn_2SbO_6:Cr^{3+}$ phosphors for light-emitting diodes. *iScience* **2021**, *24*, 102250−102277.
(52) Zhang, Q.; Liu, D.; Dang, P.; Lian, H.; Li, G.; Lin, J. Two Selective Sites Control of Cr3+-Doped ABO4 Phosphors for Tuning Ultra-Broadband Near-Infrared Photoluminescence and Multi-Applications. *Laser Photonics Rev.* **2021**, *16*, 2100459−2100464.
(53) Gao, P.; Dong, P.; Zhou, Z.; Zhang, X.; Li, Y.; Yang, J.; Li, Q.; Chen, K.; Molokeev, M. S.; Zhou, Z.; et al. Novel Far-red Phosphors $(La,Gd,Y)_2MgTiO_6:Cr^{3+}$ with Tunable Luminescence Spectra for Grow Ligh. *Chin. J. Lumin.* **2022**, *43*, 58−68.





https://doi.org/10.1021/acs.jpcc.2c02560
*J. Phys. Chem. C* 2022, 126, 9195−9206